Faraday Discussions

Accepted Manuscript

This manuscript will be presented and discussed at a forthcoming Faraday Discussion meeting. All delegates can contribute to the discussion which will be included in the final volume.

Register now to attend! Full details of all upcoming meetings: http://rsc.li/fd-upcoming-meetings

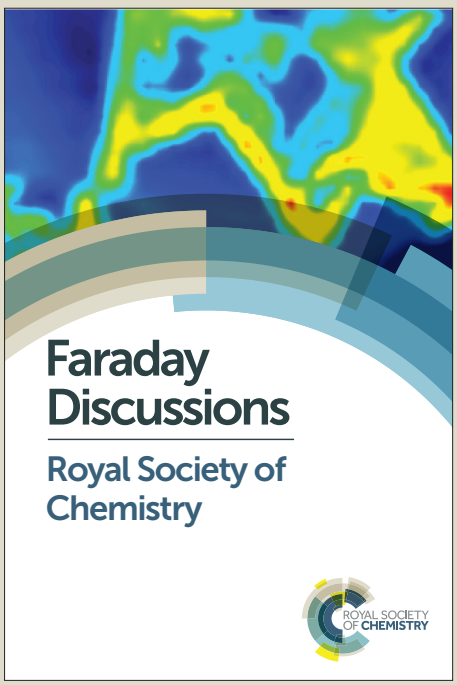

This is an *Accepted Manuscript*, which has been through the Royal Society of Chemistry peer review process and has been accepted for publication.

Accepted Manuscripts are published online shortly after acceptance, before technical editing, formatting and proof reading. Using this free service, authors can make their results available to the community, in citable form, before we publish the edited article. We will replace this *Accepted Manuscript* with the edited and formatted *Advance Article* as soon as it is available.

You can find more information about *Accepted Manuscripts* in the Information for Authors.

Please note that technical editing may introduce minor changes to the text and/or graphics, which may alter content. The journal's standard Terms & Conditions and the Ethical guidelines still apply. In no event shall the Royal Society of Chemistry be held responsible for any errors or omissions in this *Accepted Manuscript* or any consequences arising from the use of any information it contains.

ROYAL SOCIETY OF CHEMISTRY

www.rsc.org/faraday_d

Journal Name

RSCPublishing

ARTICLE

Mechanisms for CO oxidation on Fe(III)-OH-Pt interface: a DFT study

Cite this: DOI: 10.1039/x0xx00000x

Yun Zhao,[a] Guangxu Chen,[a] Nanfeng Zheng *[a] and Gang Fu* [a]

Received 00th January 2012,
Accepted 00th January 2012

DOI: 10.1039/x0xx00000x

www.rsc.org/

The full catalytic cycle that involves the oxidation of two CO molecules is investigated here by using periodic density functional calculation. To simulate the nature of $Fe(OH)_x$/Pt nanoparticles, three possible structural models, i.e. $Fe(OH)_x$/Pt(111), $Fe(OH)_x$/Pt(332) and $Fe(OH)_x$/Pt(322), are built. We demonstrate that Fe(III)-OH-Pt stepped sites readily react with CO adsorbed nearby to directly yield CO_2 and simultaneously produce coordinatively unsaturated iron sites for O_2 activation. By contrast, the created interfacial vacancy on $Fe(OH)_x$/Pt(111) prefers to adsorb CO rather than O_2, thus inhabiting the catalytic cycles of CO oxidation. We suggest that such a structure sensitivity can be understood in terms of the bond strengths of Fe(III)-OH.

Introduction

Catalytic oxidation of CO to CO_2 is believed to be one of the best-known heterogeneous processes.[1-11] On one hand, CO oxidation has been regarded as a prototypical reaction which can provide fundamental insight into the structure of the active sites at solid surface or interface; on the other hand, such a reaction bear considerable practical value in CO removal from car exhausts and the purification of hydrogen fuel in the proton exchange membrane fuel cells (PEMFCs) anode.[12] Developing an efficient strategy to achieve high performance of CO oxidation under ambient condition is highly desirable. As CO can chemisorb on the noble metal (NM) while reducible transition metal oxides (TMO) usually have relative high oxygen affinity, it was expected that combining both of them to create a TMO/NM interface could work in synergy to boost the CO oxidation. Based on this concept, numerous catalysts have been successfully developed, such as Au/TiO_2,[1,13] Rh/CeO_2,[2] Pt/FeO_x,[3-8,11] Cu/NiO[9] and $Cu/TiO_2(CeO_2)$[10,14,15] systems. Among them, Pt/FeO_x system has been extensively studied by experiment and theory, owing to its high activity at low temperature and high resistance to oxidation.[3-5] It is generally accepted that CO oxidation occurs through the Langmuir-Hinshelwood (L-H) mechanism including multiple elementary steps, such as CO and O_2 adsorption, O-O bond dissociation, and C-O bond formation. However, not all aspects of the reaction have been explored in sufficient depth, and several fundamental questions are still under heavy debate: (i) What is the nature of the Pt-FeO_x interface? (ii) What are the roles that water plays in CO oxidation? (iii) What kinds of intermediates are involved?

As previously reported, both bilayer coordinatively unsaturated O–Fe/Pt and trilayer coordinatively saturated (H)O-Fe-O/Pt interface have been proposed as active sites for CO oxidation. Based on surface science experiments and density functional theory (DFT) calculations, Fu et al. suggested that coordinately unsaturated Fe(II) (CUF) sites confined at the Pt-FeOx interface, i.e. O–Fe/Pt, show a high activity in CO oxidation under PEMFC condition.[3] DFT calculations revealed that such high reactivity might originate from the preferential adsorption of oxygen over CO on the CUF sites. It should be pointed out that low-valence ferrous is not stable in oxidative environments. For instance, Ringleb et al. showed that FeO(111)/Pt(111) would undergo strong reconstruction under 10-100 mbar partial pressure of oxygen, leading to formation of trilayer coordinatively saturated O-Fe-O/Pt film, and the latter readily converts into a hydroxyl terminated trilayer with a HO-Fe-O/Pt structure when contacts with water.[8,16] XPS results indicated that Fe present in such a trilayer film is in +3 oxidation state.[4,8,16] Experimentally, (H)O-Fe-O/Pt was found to be stable in air, but nearly not active towards CO oxidation at room temperature. [4,8]

It has been well documented that water would play versatile roles in CO oxidation. On one hand, water is generally a promoter for CO oxidation on NM surface.[17-20] Gong et al. performed DFT calculation to demonstrated that in the presence of H_2O, CO oxidation on Pt(111) began with the reaction of CO and OH, and then the resulting COOH further interact with another OH to give CO_2 and H_2O.[18] By means of inelastic neutron scattering spectroscopy, Parker further confirmed that two OH group were required for low temperature CO oxidation.[19] On the other hand, a small amount of water would inhibit CO oxidation over TMO, such as CuO, MnO_x and Co_3O_4.[21-24] Wang et al. proposed that the influence of water was so different on NM and TMO because there existed significant difference in energy barrier for movement of OH on metal and metal oxide.[24] Obviously, TMO/NM system is expected to bring more complex chemistry. On the interface of FeO/Pt(111), the reaction of CO with OH was identified experimentally by Huang et al.[16] Recent DFT calculations

by Li et al. suggested that water not only accelerated the reaction, but also promoted interfacial interactions between FeO and Pt(111).[11] Another related topic of interest is water-gas shift (WGS) reaction ($CO + H_2O \rightarrow CO_2 + H_2$), in which TMO/NM catalysts were usually employed.[10,13-15] Most evidences supported that WGS reaction occurred by an associative mechanism where CO reacted with OH derived from water dissociation, leading to formation of COOH intermediate, which further underwent dehydrogenation to generate CO_2.[10,13-15] These results indicated that the OH located at the interfaces between TMO and NM would play a crucial role in CO oxidation.

Very recently, we have successfully fabricated a series of sub-5 nm iron hydroxide-platinum hybrid nanoparticles to demonstrate a smart, collaborative Fe(III)-OH-Pt interface that is highly efficient for CO oxidation.[25] On the basis of the molecular-level characterizations (i.e. aberration-corrected STEM, EXAFS, XANES, XPS, etc.), the iron cations were proved to be present as +3, which was surrounded mainly by OH groups. Our DFT calculations and isotope labelling experiments revealed that the OH groups at the Fe(III)-OH-Pt interfaces readily reacted with CO adsorbed nearby to directly yield CO_2 and simultaneously generated coordinatively unsaturated iron sites for O_2 activation. In this contribution, we will present a comprehensive study on the fully catalytic cycle involving the oxidation of two CO molecules by using different structural models. The structure sensitivity of different interfaces will be highlighted as well.

Computational Method and Model

Spin polarization calculations are carried out by using the Vienna ab initio simulation package (VASP).[26,27] The valence electrons are described by plane wave basis sets with a cutoff energy of 400 eV, and the core electrons are replaced by the projector augmented wave pseudopotentials.[28,29] The k-points sampling for all structural models is generated following the Monkhorst-Pack procedure with a 2×3×1 mesh.

Here, we demonstrate how to build a sophisticated catalyst model that incorporates most the physical/chemical properties characterized by experiments. High resolution-STEM showed that the Pt core in $Fe(OH)_x$/Pt nanoparticles is mainly enclosed with (111) and (100) facets. It was reported previously that iron oxides film, such as FeO, Fe_2O_3 and Fe_3O_4, are able to spread over Pt(111) surface. Thus, we expect that $Fe(OH)_x$ could also deposited onto the Pt(111). Besides the flat (111) surface, two kinds of stepped surfaces, i.e. Pt(332) [n(111)×(111)] and Pt(322) [n(111)×(100)], are also taken into account to simulate the edge sites prevalent in nanoparticles. Here, $Fe_6O_{18}H_{15}$ cluster is chosen as a model for $Fe(OH)_x$, which is constructed by cutting the Fe_6O_{18} moiety from goethite FeOOH crystal and then saturating most of the outer O atoms with H atoms, giving rise to $Fe_6O_{18}H_{15}$. Such a cluster can be place on (111) terrace of the flat or stepped surfaces, resulting in three possible structural models, i.e. $Fe(OH)_x$/Pt(111), $Fe(OH)_x$/Pt(332) and $Fe(OH)_x$/Pt(322), as illustrated in Fig 1. DFT calculations shows that $Fe_6O_{18}H_{15}$ can strongly anchor on the surfaces with a binding energy of 1.05, 1.09 and 1.15 eV/Fe atom for Pt(111), Pt(332) and Pt(322), respectively. Bond valence sum (BVS) calculations show that the average valence of Fe atoms is in the range varied from 2.883 to 2.966, indicating that they are ferric species.[30,31]

Deep inspection shows that such models do reflect the structure features obtained from experimental studies:[25] (1) Structural parameters (bond distances, coordination number) of the optimized model structures can fit those from EXAFS experiments. (2) Both Bader charge analysis and valence bond simulations shows that Fe is in the +3 valence state, consistent with the XANES and XPS experiments; and (3) OH/O ratio in our model is equal to 5, close to that deduced from XPS (~4.2). (4) There are still open Pt sites on surface, consistent with the results of low energy ion scattering spectroscopy.

Table 1 Valence and structural parameters of $Fe(OH)_x$ /Pt obtained by DFT calculations and experiments

Surfaces	Metal	Valence	M-O (Å)	M-M (Å)
Pt(111)	Pt	+0.192	2.126	2.775
	Fe	+2.966	2.041	3.014
Pt(332)	Pt	+0.203	2.135	2.775
	Fe	+2.905	2.045	3.028
Pt(322)	Pt	+0.181	2.113	2.777
	Fe	+2.883	2.047	3.019
Pt nano (expt)[25]	Pt	δ+	1.99±0.01	2.761±0.001
	Fe	+3	1.97±0.02	3.01±0.02

Exchange and correlation functionals are treated within the Perdew-Burke-Ernzerhof (PBE) generalized gradient approximation (GGA).[32] Since GGA was reported to be insufficient to describe the Columbic repulsion between the Fe 3d electrons, here we adopt the GGA+U approximation with U_{eff} of 3.0 eV for Fe atoms.[3,5,33] or spin polarization calculations, the arrangement of spins on different Fe atoms remarkably influences the energies. In the structural models described above, there are two columns of Fe atoms, and three Fe atoms in each column. Our calculations show that antiferromagnetic (AFM) structures are more favourable than ferromagnetic (FM) ones, and the row-wise (RW) arrangement favour over the nearest neighbour (NN) one. Thus, all energies reported here use the RW-AFM configuration for Fe atoms.

During structural optimization, the bottom three layers of the slab are fixed at the bulk truncated position, while the top two layers and the adsorbed molecules are fully relaxed. The minimum energy reaction pathways are calculated using the nudged elastic band method. And the final transition state (TS) structures are refined by using a quasi-Newton algorithm until the Hellman-Feynman forces on each ion were lower than 0.03 eV/Å. Moreover, frequency calculations are performed to confirm the TS which have only one

imaginary frequency. The adsorption energies (ΔE_{ads}) are calculated by using equation (1):

$$\Delta E_{ads} = E_{ad/sub} - E_{ad} - E_{sub} \quad (1)$$

in which $E_{ad/sub}$, E_{ad}, and E_{sub} are the total energies of the optimized adsorbate/substrate system, the adsorbate in the gas phase, and the clean substrate, respectively.

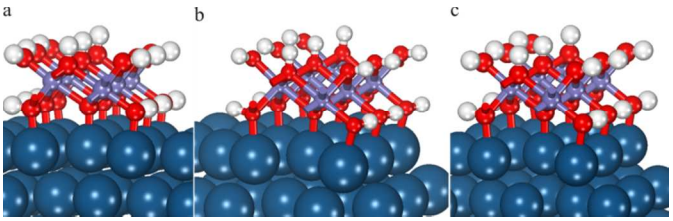

Fig. 1 The possible structural models for Fe(III)-OH-Pt interface: (a) $Fe(OH)_x$ /Pt(111), (b) $Fe(OH)_x$/Pt(332) and (c) $Fe(OH)_x$/Pt(322).

Results and discussion

1 Adsorption of CO and O_2 on $Fe(OH)_x$/Pt surfaces

To boost the low temperature CO oxidation, the key is to depress the CO adsorption and promote the adsorption of O_2. Here, we compare the adsorption energies of CO and O_2 on naked and $Fe(OH)_x$ deposited Pt surfaces, as listed in Table 2. It was reported previously that DFT/GGA method would underestimate site preference for CO adsorption on low-coordination sites on Pt(111) system, i.e. CO/Pt(111) puzzle.[34,35] Computationally, the differences in energy between top and hollow site are usually less than 0.3 eV, thus having a minor effect on following discussion. We show that CO prefers to adsorb on fcc hollow site of Pt(111) with an energy of -1.87 eV, consistent with previous works of -1.74[36] and -1.85 eV,[37] but larger than those of top site on Pt(111) (-1.64 eV). The Pt(332) and Pt(322) surfaces have five-atom and four-atom wide (111) terraces, respectively, and each unit of both of them contains one column of stepped atoms. Our calculations show that for the stepped surfaces, CO adsorbs preferentially on edge top. The calculated adsorption energy are -1.96 and -2.05 eV, which are slightly larger than that of CO adsorption on (111) plane. For O_2 adsorption on Pt(111), the most stable adsorption occurs at the bridge site with energy of -0.67 eV, in good agreement with those in the previous calculations (-0.63 ~ 0.71 eV).[11,38] Bader charge analysis shows that adsorbed O_2 is negatively charged by -0.43e, clearly indicating that an electronic rearrangement occurs after adsorption. We also consider the adsorption of O_2 on the edge sites. As shown in Table 2, the calculated adsorption energies for O_2 on the step of Pt(332) and Pt(322) are -0.53 and -0.62 eV, respectively, suggesting that molecular O_2 tend to adsorb on the flat surface. All these indicate that O_2 adsorption would be significantly poisoned by CO adsorption over metallic Pt surfaces since the latter are -1.2 ~ -1.4 eV more favourable in energy than the former, thus suppressing the low temperature CO oxidation. Indeed, our experiments have also demonstrated that without $Fe(OH)_x$ deposition, pristine Pt nanoparticles exhibited 100% CO conversion only when the temperature is high than 373K.

Bader charge analysis (Table 1) shows that the Pt atoms at the $Fe(OH)_x$/Pt interfaces are positively charged by +0.18 ~ +0.20e, indicating that significant charge transfers from Pt 5d orbital to $Fe(OH)_x$. More vacant d orbitals in Pt result in less electron dotation to the $2\pi^*$ orbitals of CO, thus weakening the CO adsorption. Actually, calculations on Fe(III)-OH-Pt interface yield a significant decrease of adsorption energy for CO (0.5 ~ 1.0 eV). Meanwhile, we find that O_2 adsorption is also inhibited at the interfaces with energy decrease of 0.2 ~ 0.3 eV. Thus, the differences between CO and O_2 adsorption are still very large, varied from 0.7 to 1.1 eV, and the situation of preferentially adsorption of CO to O_2 could not be changed even the Fe(III)-OH-Pt interfaces have been formed.

Table 2 Calculated adsorption energies for CO and O_2 on naked and $Fe(OH)_x$ deposited Pt surfaces (unit: eV)

Surface	CO	O_2
Pt(111)	-1.87 -1.74[36] -1.85[37] -1.64[11]	-0.67 -0.71[11] -0.63[38]
$Fe(OH)_x$/Pt(111)	-1.43	-0.70
Pt(332)	-1.96 -2.41[a,39] -2.43[b,39]	-0.53
$Fe(OH)_x$/Pt(332)	-1.01	-0.34
Pt(322)	-2.05 -2.41[a,39] -2.43[b,39]	-0.62
$Fe(OH)_x$/Pt(322)	-1.43	-0.31

[a] CO adsorption on Pt(211)
[b] CO adsorption on Pt(311)

2 The first CO oxidation on $Fe(OH)_x$/Pt interfaces

In WGS reaction, CO oxidation begins with the reaction of CO and OH group to form COOH species.[10,13-15] This process can be viewed as CO insertion, which is prevalent in organometallic chemistry. In our case, hydroxyl species are readily available at the interface so that the CO oxidation is also expected to be triggered by the coupling reaction between the adsorbed CO and interfacial OH. Fig. 2 displays the calculated reaction profiles of the first CO oxidation process over the $Fe(OH)_x$/Pt interfaces and the TS structures are summarized in Fig. 3. Experimentally, the exposed Pt atoms could be saturated by CO even at room temperature. Here, the state in which all open Pt sites except one are occupied by CO is defined as the zero energy reference (i). Interestingly, the adsorption energies for the last CO over different Pt surfaces are calculated to be exothermic by -0.32 ~ -1.05 eV, much lower than those of low coverage cases. Next, CO can interact with an OH group in the vicinity, leading to formation of adsorbed CO_2 (iii) directly or via COOH intermediate (ii). Our calculations show that COOH species can only be stabilized on Pt(322). This step via TS-1 is calculated to be exothermic by 0.16 eV and exhibits a barrier of 0.69 eV. Such a barriers is higher than those on FeO/Pt(111) (0.33 eV),[11] CeO_x/Cu(111) (0.41 eV),[15] but lower that on TiO_2/Au(111) (~1.1 eV).[13] After transferring the H to the neighbour OH group, COOH (iii) can convert into adsorbed CO_2 species (iv) by overcoming a

small barrier of 0.20 eV (TS-2). On $Fe(OH)_x/Pt(111)$ and $Fe(OH)_x/Pt(332)$ interfaces, COOH is not stable since H transfer from COOH to nearby OH occurs spontaneously, and adsorbed CO_2 can be directly formed with the assistance of two OH groups, i.e. TS-1′. The calculated barriers are 0.48 eV and 0.69 eV for Pt(111) and Pt(332)], respectively, with respect to CO adsorption (ii). This indicates that the OH present in flat surface, i.e. Pt(111) are more active in CO oxidation than those on stepped ones, such as Pt(332) and Pt(322). Subsequently, release of CO_2 takes place to yield a vacancy on the interface, i.e. Fe-□-Pt, with a small activation barrier of 0.16 ~ 0.32 eV.

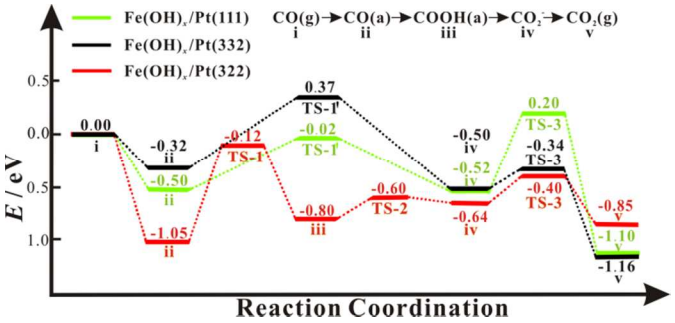

Fig. 2 The proposed reaction mechanisms for the first CO oxidation on the $Fe(OH)_x/Pt(111)$, $Fe(OH)_x/Pt(332)$ and $Fe(OH)_x/Pt(322)$ catalysts.

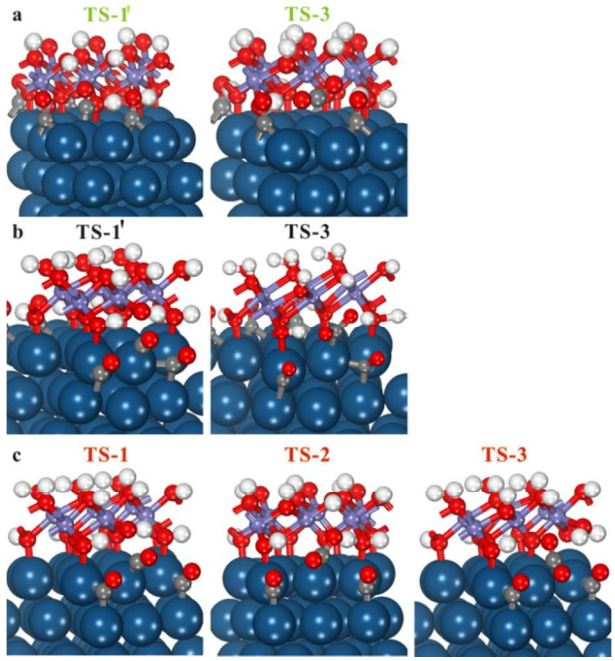

Fig. 3 Optimized TS structures for the first CO oxidation over (a) $Fe(OH)_x/Pt(111)$; (b) $Fe(OH)_x/Pt(332)$; (c) $Fe(OH)_x/Pt(322)$.

The proposed reaction mechanism can nicely account for the experimental observations. Bader analysis shows that the adsorbed CO_2 (iv) can be viewed as $CO_2^{\delta-}$ which carries significant negative charge of 0.55~0.87e. Experimentally, such species have been identified over both $CeO_x/Cu(111)$ and $CeO_x/Au(111)$ under WGS condition.[13,15] In addition, we predicts that the apparent energy barrier is in the range of 0.00 - 0.37 eV for CO oxidation by Fe(III)-OH-Pt interface, in good agreement with experimental value (0.16 eV).[25] Isotope labelling experiments revealed that in the absence of O_2, CO is able to react with the interfacial Fe(III)-OH-Pt sites to yield CO_2, further supporting our mechanism.[25] This finding casts some doubt on the well-accepted assumption that the CO oxidation by FeO_x/Pt should start from O_2 activation.[5,11]

3 Competitive adsorption of CO and O_2 on Fe-□-Pt

The created interfacial vacancy can be competitively adsorbed by CO and O_2, as shown in Fig. 4. Bader charge analysis reveals that the Pt site under as-formed vacancy at the interface is positively charged by +0.15 ~ +0.19e. Accordingly, the adsorption energies for CO are predicted to be -1.30, -0.87 and -1.60 eV for Pt(111), Pt(332) and Pt(322), respectively, lower than those on naked Pt surfaces. On the other hand, BVS analysis shows that the average valence of Fe atoms reduces to +2.05 ~ +2.22. Low valence iron is expected to be preferential to adsorb and activate the O_2 molecule. It should be pointed out that upon O_2 adsorption, a proton would spontaneously transfer from the nearby water to make OOH species. For Pt(111), the adsorption energy of O_2 is exothermic by -1.18 eV, while the stepped surfaces lead to more stable adsorption with energies of -1.34 eV and -1.70 eV for Pt(332) and Pt(322), respectively. Charge and spin analysis show that the O-O groups are negatively charged by -1.20 ~ -1.24e; meanwhile, the magnetic moments on O atoms are completely quenched. Thus, the enhancement of O_2 adsorption can be attributed to the strong electrostatic attraction between $O_2^{\delta-}$ and Fe cations. From Fig. 4, we can see that the adsorption of O_2 is preferential to CO on stepped sites; whereas CO adsorption favours over O_2 (-1.30 vs -1.18 eV) on the terrace. Such a structure sensitivity might origin from the difference in bond strength of Fe(III)-OH. Our calculations show that the strength of Fe(III)-OH decreases in the order -3.30 eV {Pt(111)} > -3.61 eV {Pt(322)} ≈ -3.68 eV {Pt(332)}. A weak Fe(III)-OH bond results in a high activity for the reaction of CO and OH, while a relative low adsorption energy for O_2. In this regard, the vacancies on stepped sites can be efficiently healed by oxygen; while Fe(III)-□-Pt(111) site still suffers from the CO poisoning. This can explain why trilayer (H)O-Fe-O/Pt structure only exhibits low activity for CO oxidation under room temperature.[4,7,8] In addition, the role of nearby H_2O played should also be highlighted as it could provide H to generate OOH species. Computationally, the adsorption of H_2O is not so strong that it should be replenished by feed gas, accounting for the fact that the reactivity of CO oxidation only maintained in the humid air.[25]

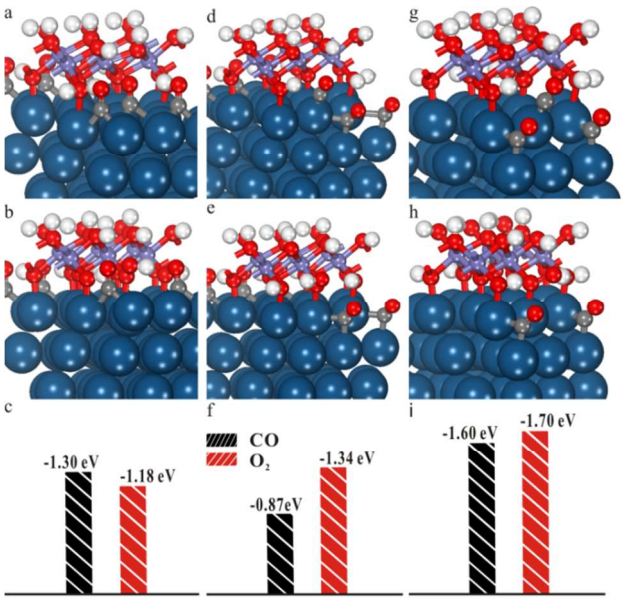

Fig. 4 The adsorption structures of CO and O_2, respectively, on the created interfacial vacancies. (a, b) a Pt(111) surface. (d, e) a Pt(332) surface. (g, h) a Pt(322) surface, (c, f and i) The adsorption energies corresponding to (a-b, d-e and g-h).

4 Mechanism of the second CO oxidation

Next, we will investigate the second CO oxidation continuing from the interfacial vacancy (v), as shown in Fig. 5. And the optimized TS structures illustrate in Fig. 6. For simplicity, here we limit our scope on the Pt(322) surface. By adsorbing O_2 and CO, the interface has been 'saturated' again (vii), with an exothermicity of -1.54 eV. In following reaction, two possible pathways are considered, namely Path A and Path B. The former involves the coupling between OOH and CO via TS-4 with a barrier of 1.38 eV. This step is calculated to be strongly exothermic by -3.82 eV, leading to the formation of CO_2 and the recovery of Fe(III)-OH-Pt interface (i), thus completing the catalytic cycle. On the other hand, the second CO oxidation can also begin with the reaction of CO + OH, i.e. Path B, which is similar to the mechanism for the first CO oxidation. Again, COOH intermediate cannot be located, and directly transforms into $CO_2^{\delta-}$ species together with adsorb H_2O_2 (viii) via TS-5 with a relative low barrier of 0.73 eV. This indicates that interfacial OH species is more active than the interfacial OOH towards CO oxidation. Subsequently, $CO_2^{\delta-}$ can overcome a 0.62 eV barrier (TS-6) to liberate a CO_2 and yield a new vacancy (ix). If the vacancy could be occupied by water (x), the HO-OH bond can be readily broken with the assistance of the water. Only a small barrier, 0.34 eV, is require to overcome TS-7, which is followed by an exothermicity of -1.24 eV to the formation of two OH groups, eventually recovering the Fe(III)-OH-Pt interface (i) yet. We suggest that these two pathways are competitive under working condition because the water adsorption on the vacancy (x) is rather weak (-0.38 eV), downplaying the significance of Path B. Nevertheless, we still anticipate that increasing water pressure might favour Path B over Path A. Another interesting finding is that H_2O_2 species are generated along the Path B. This let us recall the well-known Fenton system, i.e. Fe(II)+H_2O_2,[40,41] which is usually used to oxidation of organic contaminants to carbon dioxide under ambient condition. We expect that Fe(III)-OH-Pt could also show a great promise in the catalytic oxidation of hydrocarbon.

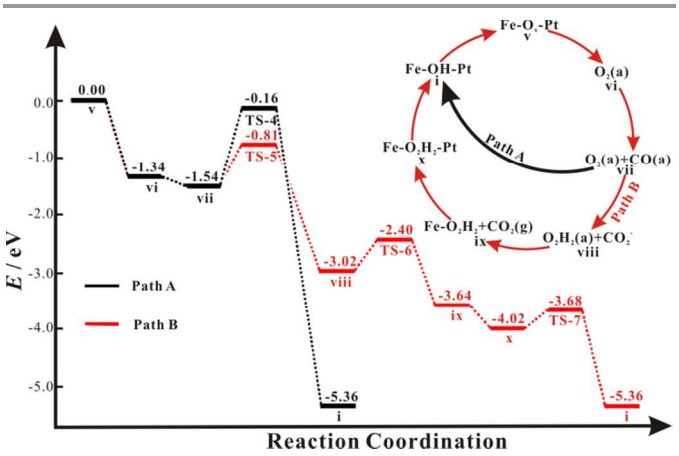

Fig. 5 Possible pathways for the second CO oxidation over $Fe(OH)_x$/Pt(332).

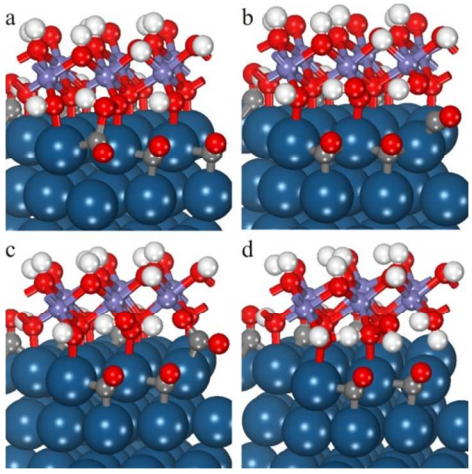

Fig. 6 Optimized TS structures for the second CO oxidation along the energy profiles. (a)TS-4; (b) TS-6; (c) TS-7 and (d) TS-8.

Conclusions

Here we present a theoretical investigation on the full catalytic cycle of CO oxidation by Fe(III)-OH-Pt interface. The main conclusions can be summarized as follows:

(1) Our calculations show that CO oxidation could begin with the coupling between CO and OH with barriers of 0.48 ~ 0.93 eV. This indicates that OH present in Fe(III)-OH-Pt is rather active, liable to oxidizing CO into CO_2.

(2) CO oxidation is found to be a structure sensitive reaction. We show that the performance of different exposing surfaces is depended on the bond strength of Fe(III)-OH. A weak Fe(III)-OH bond at $Fe(OH)_x$/Pt(111) interface results in a high activity towards CO+OH reaction; however, renders the interfacial vacancy preferentially occupied by CO, inhibiting the activation of O_2. On the other hand, $Fe(OH)_x$ together with Pt

edge site is able to effectively activate both CO and O_2, thus enhancing the low-temperature reactivity of CO oxidation.
(3) In addition, the roles that the adsorbed water plays in adsorption and activation of O_2 have been shed light on. On one hand, it can stabilize O_2 adsorption by forming OOH species; on the other hand, the O-O bond breaking can be facilitated by the coexistence of water.
(4) We show that during the oxygen evolution, H_2O_2 species can be formed such that Fe(III)-OH-Pt interface might play a crucial role in catalytic oxidation of hydrocarbon under ambient condition.

We believe that such detailed mechanistic understanding provides new insights on roles of the interfacial OH, which will shed light on the design of more efficient TMO/NM catalysts.

Acknowledgements

We thank the financial support from the Ministry of Science and Technology of China (2011CB932403), the National Nature Science Foundation of China (21131005, 20925103, 21373167, 21033006, 21133004, 21333008) and the Fundamental Research Funds of Central Universities. And G. Fu thanks Shanghai Supercomputer Center (SSC) to provide computational resource.

Notes and references

[a] State Key Laboratory for Physical Chemistry of Solid Surfaces, Collaborative Innovation Center of Chemistry for Energy Materials, College of Chemistry and Chemical Engineering, Xiamen University, Xiamen 361005, China

† Footnotes should appear here. These might include comments relevant to but not central to the matter under discussion, limited experimental and spectral data, and crystallographic data.
Electronic Supplementary Information (ESI) available: [details of any supplementary information available should be included here]. See DOI: 10.1039/b000000x/

(1) I. X. Green, W. Tang, M. Neurock and J. T. Yates, *Science*, 2011, **333**, 736.
(2) W. Song, A. P. J. Jansen and E. J. M. Hensen, *Faraday Discuss.*, 2013, **162**, 281.
(3) Q. Fu, W. X. Li, Y. X. Yao, H. Y. Liu, H. Y. Su, D. Ma, X. K. Gu, L. M. Chen, Z. Wang, H. Zhang, B. Wang and X. H. Bao, *Science*, 2010, **328**, 1141.
(4) Y.-N. Sun, L. Giordano, J. Goniakowski, M. Lewandowski, Z.-H. Qin, C. Noguera, S. Shaikhutdinov, G. Pacchioni and H.-J. Freund, *Angew. Chem. Int. Ed.*, 2010, **122**, 4520.
(5) B. Qiao, A. Wang, X. Yang, L. F. Allard, Z. Jiang, Y. Cui, J. Liu, J. Li and T. Zhang, *Nat. Chem.*, 2011, **3**, 634.
(6) Y. Lei, M. Lewandowski, Y.-N. Sun, Y. Fujimori, Y. Martynova, I. M. N. Groot, R. J. Meyer, L. Giordano, G. Pacchioni, J. Goniakowski, C. Noguera, S. Shaikhutdinov and H.-J. Freund, *ChemCatChem*, 2011, **3**, 671.
(7) L. Giordano, M. Lewandowski, I. Groot, Y.-N. Sun, J. Goniakowski, C. Noguera, S. Shaikhutdinov, G. Pacchioni and H.-J. Freund, *J. Phys. Chem. C*, 2010, **114**, 21504.
(8) F. Ringleb, Y. Fujimori, H.-F. Wang, H. Ariga, E. Carrasco, M. Sterrer, H.-J. Freund, L. Giordano, G. Pacchioni and J. Goniakowski, *J. Phys. Chem. C*, 2011, **115**, 19328.
(9) L.-Y. Gan and Y.-J. Zhao, *J. Phys. Chem. C*, 2012, **116**, 16089.
(10) H. Y. Kim and P. Liu, *ChemCatChem*, 2013, **5**, 3673.
(11) X.-K. Gu, R. Ouyang, D. Sun, H.-Y. Su and W.-X. Li, *ChemSusChem*, 2012, **5**, 871.
(12) G. J. K. Acres, J. C. Frost, G. A. Hards, R. J. Potter, T. R. Ralph, D. Thompsett, G. T. Burstein and G. J. Hutchings, *Catal. Today*, 1997, **38**, 393.
(13) J. A. Rodriguez, S. Ma, P. Liu, J. Hrbek, J. Evans and M. Pérez, *Science*, 2007, **318**, 1757.
(14) J. A. Rodriguez, J. Graciani, J. Evans, J. B. Park, F. Yang, D. Stacchiola, S. D. Senanayake, S. Ma, M. Pérez, P. Liu, J. F. Sanz and J. Hrbek, *Angew. Chem. Int. Ed.*, 2009, **48**, 8047.
(15) K. Mudiyanselage, S. D. Senanayake, L. Feria, S. Kundu, A. E. Baber, J. Graciani, A. B. Vidal, S. Agnoli, J. Evans, R. Chang, S. Axnanda, Z. Liu, J. F. Sanz, P. Liu, J. A. Rodriguez and D. J. Stacchiola, *Angew. Chem. Int. Ed.*, 2013, **52**, 5101.
(16) L. Xu, Z. Wu, Y. Zhang, B. Chen, Z. Jiang, Y. Ma and W. Huang, *J. Phys. Chem. C*, 2011, **115**, 14290.
(17) J. Bergeld, B. Kasemo and D. V. Chakarov, *Surf. Sci.*, 2001, **495**, L815.
(18) X.-Q. Gong, P. Hu and R. Raval, *J. Chem. Phys.*, 2003, **119**, 6324.
(19) S. F. Parker, *Chem. Commun.*, 2011, **47**, 1988.
(20) R. Caporali, S. Chansai, R. Burch, J. J. Delgado, A. Goguet, C. Hardacre, L. Mantarosie and D. Thompsett, *Appl. Catal. B*, 2014, **147**, 764.
(21) G. Y. Wang, W. X. Zhang, Y. C. Cui, H. L. Lian, D. Z. Jiang and T. H. Wu, *Chin. J. Catal.*, 2001, **22**, 408.
(22) H. Zou, X. Dong and W. Lin, *Appl. Surf. Sci.*, 2006, **253**, 2893.
(23) D. Gamarra and A. Martínez-Arias, *J. Catal.*, 2009, **263**, 189.
(24) H.-F. Wang, R. Kavanagh, Y.-L. Guo, Y. Guo, G.-Z. Lu and P. Hu, *Angew. Chem. Int. Ed.*, 2012, **51**, 6657.
(25) G. Chen, Y. Zhao, G. Fu, P. N. Duchesne, L. Gu, Y. Zheng, X. Weng, M. Chen, P. Zhang, C.-W. Pao, J.-F. Lee and N. Zheng, *Science*, 2014, **344**, 495.
(26) G. Kresse and J. Hafner, *Phys. Rev. B*, 1993, **48**, 13115.
(27) G. Kresse and J. Furthmüller, *Phys. Rev. B*, 1996, **54**, 11169.
(28) P. E. Blöchl, *Phys. Rev. B*, 1994, **50**, 17953.
(29) G. Kresse and D. Joubert, *Phys. Rev. B*, 1999, **59**, 1758.
(30) I. D. Brown and D. Altermatt, *Acta Crystallogr. Sect. B*, 1985, **41**, 244.
(31) N. E. Brese and M. O'Keeffe, *Acta Crystallogr. Sect. B*, 1991, **47**, 192.
(32) J. P. Perdew, K. Burke and M. Ernzerhof, *Phys. Rev. Lett.*, 1996, **77**, 3865.
(33) L. Giordano, G. Pacchioni, J. Goniakowski, N. Nilius, E. D. L. Rienks and H.-J. Freund, *Phys. Rev. B*, 2007, **76**, 075416.
(34) R. A. Olsen, P. H. T. Philipsen and E. J. Baerends, *J. Chem. Phys.*, 2003, **119**, 4522.
(35) Y. Yeo, L. Vattuone and D. King, *J. Chem. Phys.*, 1997, **106**, 392.
(36) K. Doll, *Surf. Sci.*, 2004, **573**, 464.
(37) F. Abild-Pedersen and M. P. Andersson, *Surf. Sci.*, 2007, **601**, 1747.
(38) Z. Yang, J. Wang and X. Yu, *Phys. Lett. A*, 2010, **374**, 4713.
(39) H. Orita, N. Itoh and Y. Inada, *Surf. Sci.*, 2004, **571**, 161.

(40) C. Walling, *Acc. Chem. Res.*, 1975, **8**, 125.
(41) L. Chen, J. Ma, X. Li, J. Zhang, J. Fang, Y. Guan and P. Xie, *Environ. Sci. Technol.*, 2011, **45**, 3925.